MAM15(2) 09021 1/6 03/02/09 11:56 am REVISED PROOF log no. MAM09021

Microsc. Microanal. 15, 93–98, 2009
doi:10.1017/S1431927609090217

Microscopy AND Microanalysis

Detector Solid Angle Formulas for Use in X-Ray Energy Dispersive Spectrometry

Nestor J. Zaluzec*

Argonne National Laboratory, Electron Microscopy Center, Materials Science Division Bldg. 212, 9700 S. Cass Ave., Argonne, IL 60439

Abstract: With the advent of silicon drift X-ray detectors, a range of new geometries has become possible in electron optical columns. Because of their compact size, these detectors can potentially achieve high geometrical collection efficiencies; however, using traditional approximations detector solid angle calculations rapidly break down and at times can yield nonphysical values. In this article we present generalized formulas that can be used to calculate the variation in detection solid angle for contemporary Si(Li) as well as new silicon drift configurations.

Key words: solid angle, SDD, Si(Li), X-ray detectors, EDS, XEDS, collection efficiency

Introduction

The lithium-drifted silicon [Si(Li)] X-ray energy dispersive spectrometer has made countless contributions toward understanding the elemental composition of specimens in a wide range of instruments and fields since its first use in electron microscopes in 1968 (Fitzgerald et al., 1968). In the last decade an updated technology, namely the silicon drift detector (SDD), has entered the microanalysis arena and is opening up new avenues of characterization of materials in the electron microscope (Gatti & Rehak, 1984; Bertuccio et al., 1992; Iwanczyk et al., 1996; Zaluzec, 2004; Kotula et al., 2008).

Regardless of which of these two systems is employed for elemental microanalysis, one factor that governs the ability of a detector to measure a signal is its collection efficiency. This parameter is simply a measure of the fraction of signal collected by a detector relative to that which is emitted from the specimen. There are a number of factors that control this efficiency, some of which owe their nature to the physics of the X-ray generation, absorption, and fluorescence processes; these latter are independent of the detector and depend only upon the X-ray excitation parameters and the elemental composition of the sample (Zaluzec, 1979; Goldstein et al., 1992).

There are two additional factors that relate directly to the detector construction and geometry. The first is the relative energy detection efficiency (ε), which is a measure of the ability to detect an X-ray as a function of its energy and depends greatly upon detector fabrication parameters, while the second is the geometrical collection efficiency (Zaluzec, 1979).

Figure 1 shows the calculated variation in energy detection efficiency for typical Si(Li) and SDD systems. At the low energy end ($<$1 keV), ε is relatively poor due to absorption of incident X-rays in the environmental isolation window(s) of the detector, reducing their detected intensity. At intermediate energies (1–10 keV) ε approaches 100%, while at the higher energy end ($>$15 keV) we observe a decrease in ε due to the transmission losses of the finite detector thickness. The SDD suffers more in this high-energy regime owing to the fact that its thickness (typically ~0.35 mm) is nearly one-tenth that of the conventional Si(Li) detector thickness (~3 mm). At the low energy end, the detailed fabrication of the environmental isolation window (calculated here for 100 nm of pyrolene) as well as the various electrical contact films (~20 nm Au) and a Si dead layer (~100 nm) control the efficiency of detection. While the Si(Li) detector has a significantly increased detection efficiency in the higher energy regime (~3× at 20 keV), the two detectors have similar performances below ~10 keV.

The major advantage of the SDD systems over Si(Li) detectors rests not in their relative energy detection efficiencies (ε shown in Fig. 1), but rather in their ability to handle high-count-rate experiments ($>$250 kcps) compared to the performance of Si(Li) systems (Zaluzec, 2004; Kotula et al., 2008). This high-count-rate performance of the SDD may be preferred for many experiments instead of the higher detection efficiency of the conventional Si(Li) detector. At the same time, the physical construction of the SDD that is directly responsible for its poorer high-energy performance (i.e., its small thickness) lends itself to fabrication in a

Received October 2, 2008; accepted January 6, 2008
*E-mail: Zaluzec@aaem.amc.anl.gov

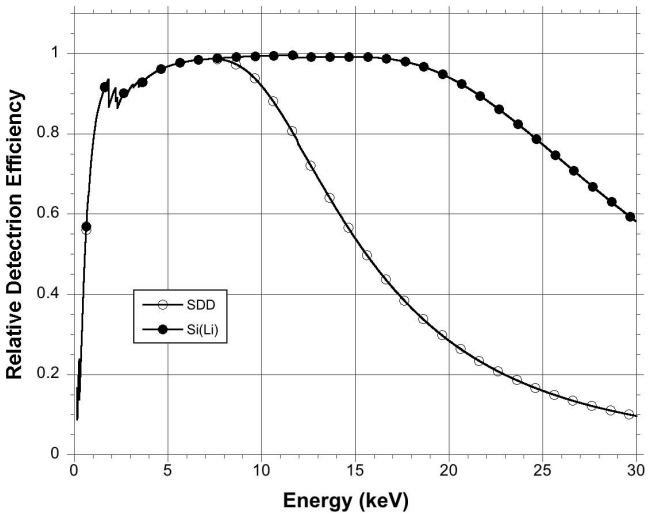

Figure 1. Calculated relative detection efficiency as a function of X-ray photon energy for Si(Li) and SDD detectors. Detector parameters: Pyrolene window ~ 100 nm, Au electrical contacts ~ 20 nm, Si dead layer ~ 100 nm, 3 mm Si(Li) thickness, 0.35 mm SDD thickness.

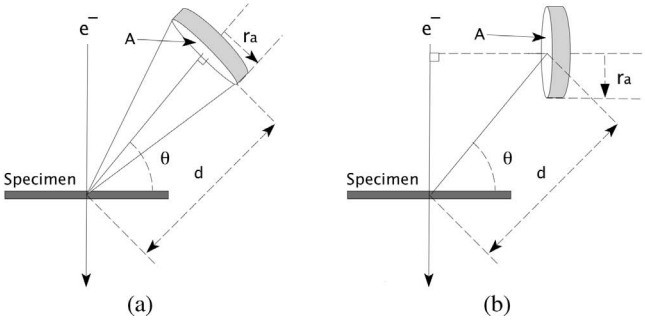

Figure 2. a: Simple off-axis geometry illustrating detector parameters commonly used in solid angle calculations. The incident beam is indicated by e^-, the active detector area is A, and the specimen-to-detector distance is d. In this illustration the detector is tilted off-axis from the incident electron beam at an elevation angle of θ relative to the specimen surface. The surface normal of the detector is aligned toward the incident beam/specimen interaction point. **b:** Illustrating a detector configuration whose surface normal is aligned perpendicular to the optic axis.

number of potentially efficient shapes and sizes. These configurations have numerous forms: from simple circular cylinders, to arrays of space filling hexagons, to novel annular configurations. These shapes and their relationship to the specimen control the geometrical collection efficiency of the detector. This collection efficiency parameter is termed the detector subtending solid angle and is measured in steradians. In the absence of all deleterious effects, an ideal detector for a thin specimen would subtend a geometrical collection solid angle of 4π steradians (a sphere completely surrounding the specimen). In practice no one has succeeded in constructing even a hemispherical X-ray detector (2π sr). Existing commercial detectors subtend significantly smaller values that, depending upon the specific configuration of the detector and the instrument, can range from 0.0001 to ~0.5 sr.

To assess the benefits of novel detector arrangements, specifically those afforded by SDD systems, it is important to correctly calculate the solid angle of any proposed detector configuration. This is particularly so when we are considering designs that might be amenable for use in aberration-corrected ultrahigh resolution electron optical columns, where detectors of small size and close proximity to the specimen are anticipated.

Calculation of Detector Solid Angle

The conventional method for calculating the nominal subtending solid angle of a detector is to compare its active detection area to the equivalent surface area of a sphere nominally located at the same radial distance from the specimen. To calculate the solid angle (Ω), one simply takes the surface area (S) of the equivalent bounding sphere divided by the square of its radius (R):

$$\Omega = \frac{S}{R^2}. \tag{1}$$

While this is an exact equation, the typical approximation made in the microanalysis community is to replace S by A, the active area of the detector, which is collecting the X-ray signal, and to replace R by d, the radial specimen-to-detector distance. In most electron column instruments, the detector axis is aligned along a radius vector extending from the excited volume. In addition, the detector axis is generally tilted with respect to the incident beam axis. This last step is done to avoid a situation where the detector may block the incident radiation, as illustrated in Figure 2a. Furthermore, if the detector system is not optimally designed, then its surface normal may not be aligned parallel to a radius vector (as illustrated Fig. 2b). Hardware in the immediate vicinity of the specimen limits the closest approach (d) that a given detector design can achieve before it collides with the specimen, its stage, or some electron optical component. Typically the value of A for commercial detectors varies from 10 to 50 mm^2, while d can vary from 10 to as much as 100 mm. For small detectors and large distances, the approximation for calculating the solid angle, alluded to above, is reasonable; however, it is important to realize that using equation (1) with these substitutions is only an approximation, and the errors compound as A increases and d decreases, leading to nonphysical results if carried too far.

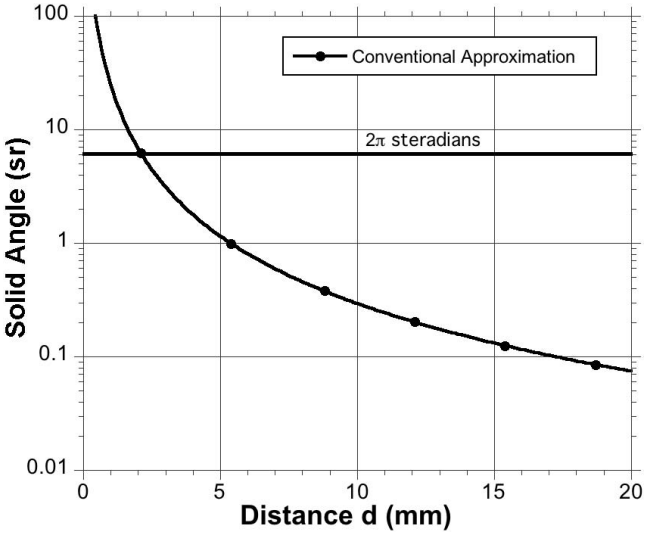

Figure 3. Solid angle variation as a function of distance using equation (1) but incorrectly substituting the active area A of the detector for S and d the specimen-to-detector distance for R. These calculations are performed for a 30 mm^2 detector. Note: Values of the solid angle greater than 2π steradians exceed physical maximums.

This is illustrated in Figure 3, where we plot the solid angle calculated when substituting A and d in equation (1), for a 30 mm^2 active area detector as a function of specimen-to-detector distance. The physical maximum for such a half-plane detector is 2π (~6.28) steradians, which would correspond to a perfect hemispherical detector resting on a specimen collecting all X-rays emitted from its surface. As one can observe, nonphysical values well in excess of 2π sr rapidly develop.

While equation (1) is physically as well as mathematically correct, the error illustrated in Figure 3 comes from equating the surface area of a sphere with that of the active area of the detector and its radius to the specimen-detector distance. To correct this, one must reformulate the solid angle formulas, taking into account the relationship of the shape of the detector and how it relates to an equivalent bounding spherical volume. This relationship is illustrated in Figure 4. Here d is the radial distance from the emission point to the normal of the detector surface, while r_a is the radius of the active area of the detector. Our problem now reduces to calculating the surface area of a sphere cut by a plane (the detector active surface) whose normal is parallel to its radius vector. To continue, we will tacitly assume that the detector is circular in cross section or, equivalently, that its active area determined by a well-defined collimator at the front of the detector, which is circular in cross section and has a radius of r_a. The surface area of a sphere of radius R bounded by the plane circular section as illustrated in Figure 4 can be shown to be:

$$S = 2\pi R(R - d) = 2\pi(r_a^2 + d^2 - d\sqrt{r_a^2 + d^2}), \qquad (2)$$

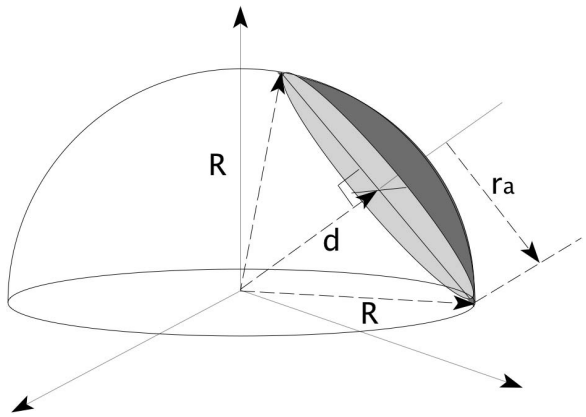

Figure 4. The geometry of a bounded spherical section, where the detector active area is represented by a plane section of circular cross section through a sphere. Here the active area is defined by its radius r_a, which is positioned at a distance d from the specimen. The distance d is measured normal to the detector surface and along a radius to the point of X-ray generation on the specimen. R is the effective radius of the subtending sphere.

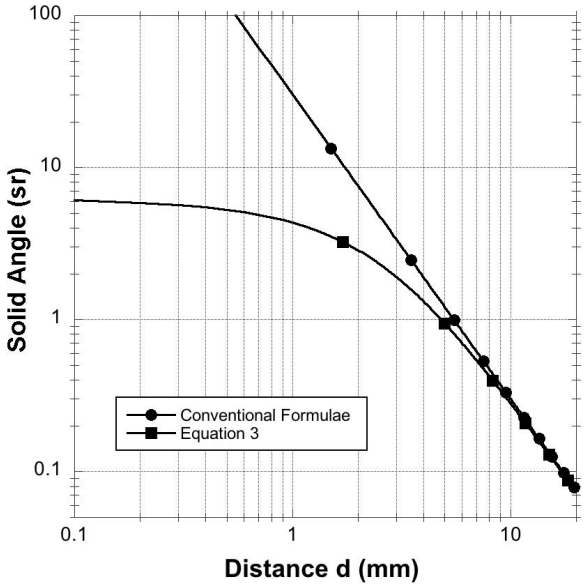

Figure 5. Comparison of the solid angle as a function of distance for a 30 mm^2 active area detector calculated using the conventional approximation and equation (3). The divergence becomes significant at distances below ~10 mm.

and the solid angle formulas then become

$$\Omega = \frac{S}{R^2} = \frac{2\pi(r_a^2 + d^2 - d\sqrt{r_a^2 + d^2})}{r_a^2 + d^2}. \qquad (3)$$

Equation (3) is plotted in Figure 5, for a 30 mm^2 detector as a function of distance, and now asymptotically converges to

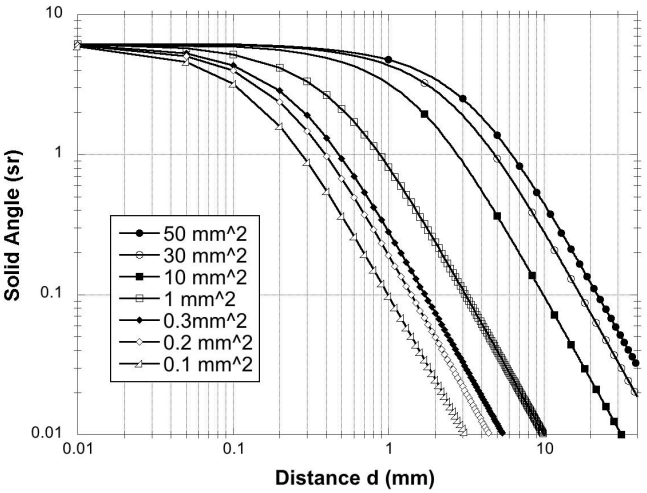

Figure 6. Variation in calculated solid angle with distance for detector active areas ranging from 0.1 to 50 mm^2.

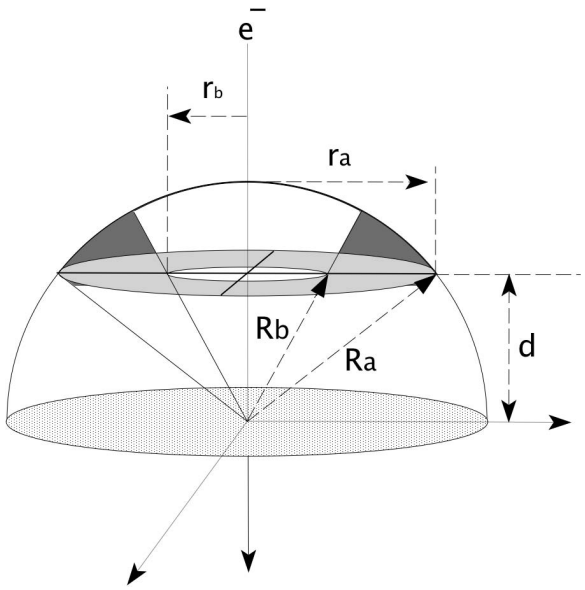

Figure 7. The geometry of an annular detector that is aligned along the electron optical axis (e^-), the parameters r_a and r_b are, respectively, the outer and inner radii of the active area of the annulus (or equivalently the radii defined by any collimation), d is the normal distance to the plane defined by the active detector surface, R_a and R_b are the effective radius of the bounding spheres intersecting at r_a and r_b .

2π steradians, which is the solid angle of a hemisphere. For detector-to-specimen distances (d) of more than 15 mm, the error in calculated solid angle is $\leq$3% between the approximation and the full calculation. However, using the incorrect formulation introduces significant errors when distances d become less than $\sim$10 mm and rising to $>$100% when $d < 3$ mm. Owing to their small size, this latter regime is where SDD detectors can contribute the most to new analytical instrumentation, and thus the use of the correct formulas is essential.

We also see that equation (3) is independent of the detector elevation angle (θ of Fig. 2a) so long as the detector surface normal (or the collimator normal) is radially aligned, and there are no obstructions in the X-ray collection beam path. If the normal to detector plane or its collimator is not radial but instead configured as is illustrated in Figure 2b, then a correction to equation (3) is necessary. To first order the correction would be to replace r_a and d in equation (3) by r_a^* and d^* with the following definitions:

$$r_a^* = r_a \cos(\theta) \tag{4}$$

and

$$d^* = d - r_a \sin(\theta). \tag{5}$$

This in effect reduces the cross-sectional area of the detector and further lowers the effective solid angle, the reduction becoming greater as the angle increases.

Returning to the optimum geometry of Figure 2a, we next explore the variation of solid angle as a function of distance for a range of detectors from a large detector of active area of 50 mm^2 ($r_a = 3.98$ mm) to a hypothetical ultrasmall detector of 0.1 mm^2 ($r_a = 0.18$ mm). These calculations are shown in Figure 6. Upon inspection, it is interesting to note that one can find a configuration of detector size and distance that attains a solid angle of 1 sr or better under a variety of conditions. While very large detectors are easy to handle, their physical size limits their use in modern high resolution electron microscopes due to the limited space surrounding the specimen. With the refinement of fabrication technology, it is interesting to speculate on the feasibility of creating ultrasmall detectors that can be inserted into the gap of an electron microscope between the sample and any lens pole pieces and still achieve high collection efficiency. From Figure 6, we see that a 0.3 mm^2 detector ($r_a = 0.3$ mm) can achieve a 1 sr collection efficiency when positioned $\sim$0.4 mm from the region of interest. These are dimensions that can be reasonably explored using MEMS devices and micromanipulators to insert and remove items in between the pole pieces of an electron microscope, as is now routinely done in focused ion beam instruments. While detectors of this ultrasmall size are currently not commercially available, it would be interesting to explore their potential, particularly in *in situ*/environmental or aberration-corrected instruments, where space is extremely limited and the availability of X-ray microanalytical instrumentation is meager.

Extending our formalism, we next consider an annular detector geometry. Here a detector having a centralized hole (to permit the passage of the incident electron beam) is placed directly above the specimen as illustrated in Figure 7.

This geometry is similar to that used in many solid state backscattered detectors used in scanning electron microscopes (SEM), and their equivalent using SDD technology is being developed by a number of commercial organizations (PNSenors,[a] Bruker-AXS,[b] SIINanotechnology USA;[c] Kotula et al., 2008).

Defining the inner radius of the annular detector as r_b and the outer radius as r_a as shown in Figure 7, we find that the equivalent spherical surface area of such an annular detector is given by

$$S = S_a - S_b = 2\pi[(r_a^2 + d^2 - d\sqrt{r_a^2 + d^2}) - (r_b^2 + d^2 - d\sqrt{r_b^2 + d^2})] \quad (6)$$

and the solid angle relationship becomes

$$\Omega = \frac{S_a}{R_a^2} - \frac{S_b}{R_b^2} = 2\pi\left[\frac{(r_a^2 + d^2 - d\sqrt{r_a^2 + d^2})}{r_a^2 + d^2} - \frac{(r_b^2 + d^2 - d\sqrt{r_b^2 + d^2})}{r_b^2 + d^2}\right]. \quad (7)$$

As the inner radius $r_b \to 0$, equation (7) reduces to equation (3).

While the presence of a centralized "hole" in the detector facilitates alignment with the optical axis of the instrument, its consequence is to decrease the total effective solid angle. We explore this relationship next in Figure 8, which plots the solid angle of an annular detector for a fixed outer radius ($r_a = 5$ mm) and variable inner radius ($0 \leq r_b \leq 3$ mm). The decrease in Ω as r_b increases is not unexpected because we are effectively removing the critical active detector area. Interestingly, we find that there is an optimum distance for a given set of parameters that maximizes the solid angle and this maximum is purely a function of r_b and d for a given outer radius r_a. For practical dimensions of a few millimeters, this maximum occurs near $r_b \sim d$.

Commercial annular detectors at the present time are not perfect annular rings as presumed for the above formulation, but rather are fabricated as arcs of rings, thus the values calculated using equation (7) needs to be reduced by the areal fraction of inactive arc length F. This is a simple multiplicative term resulting in the following relationship:

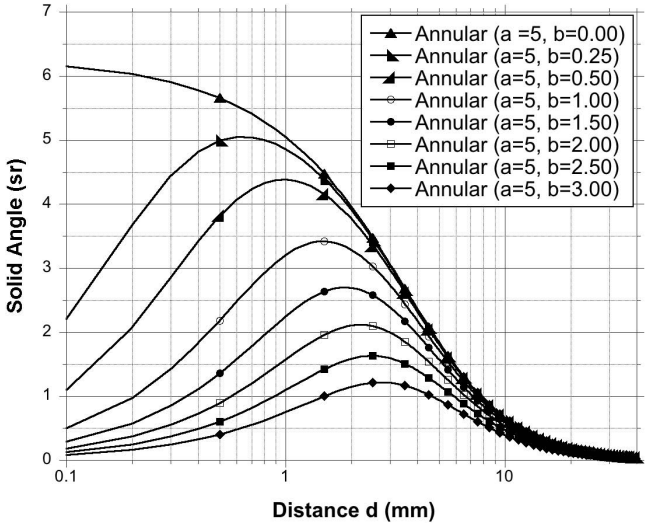

Figure 8. Calculated variation in solid angle for annular detectors as a function of distance from equation (7). Outer radius ($r_a = 5$ mm); inner radius ($0 \leq r_b \leq 3$ mm); the curve $r_b = 0$ represent a perfect hemispherical detector.

$$\Omega = (1 - F) * \left(2\pi\left[\frac{(r_a^2 + d^2 - d\sqrt{r_a^2 + d^2})}{r_a^2 + d^2} - \frac{(r_b^2 + d^2 - d\sqrt{r_b^2 + d^2})}{r_b^2 + d^2}\right]\right). \quad (8)$$

Depending upon the design of the detector, F may be as high as 0.25.

An interesting regime to explore is an annular geometry when the detector distance d is less than ~4 mm. This would be a configuration useful in a high resolution SEM or in an analytical transmission/scanning transmission electron microscope. From Figure 8, we see that solid angles of 1 sr or greater can be realized in this geometry. The merits of this become obvious when one compares the calculated solid angles with that typical of conventional off-axis Si(Li) detectors installed in such instruments. Typical conventional values can vary from 0.1 to 0.3 sr, and so an annular detector potentially would yield a 3–10 fold improvement in signal.

An additional consideration, which will also become significant in these new geometries, is detector collimation. When this new generation of detectors is interfaced to an instrument, their immediate proximity to the specimen may preclude the installation of traditional collimators. The purpose of a collimator is to restrict the collection solid angle, which is defined by the penumbra of the detector active area and any collimator edges (Zaluzec, 1979). This is a measure of the angular view of the detector to any point along its line-of-sight path. A large collection solid angle can result in the detection of systems peaks (i.e., the detec-

[a]PNSensor, commercial developer of SDD multielement detector arrays (http://www.pnsensor.de).
[b]Bruker-Axs, commercial developer of SDD multielement detector systems (http://www.bruker-axs.de).
[c]SII Nanotechnology USA, commercial developer of SDD multielement detector arrays (http://www.siintusa.com).

tion of X-ray signal generated by secondary sources in regions far away from the primary electron-excited volume). Traditionally, in collimator design one tries to minimize collection solid angle, while maximizing the subtending solid angle. It will be a challenging task to design and fit collimators in some annular geometries; this may become a limiting factor in reducing the detection of systems peaks for particular configurations.

Conclusions

We have reformulated an equation for calculating the solid angle of X-ray detectors for a number of geometries that overcomes the limitations of approximations frequently used by the microanalysis community. Using this reformulation we have seen that opportunities exist for the development of new detector configurations, which range from ultrasmall to annular geometries, and can achieve collection efficiencies approaching several sr. In particular we speculate on the development of ultrasmall detectors for use in high resolution, *in situ* and analytical electron microscope environment, where space surrounding the specimen is frequently at a premium yet microanalytical resources are limited or sometimes nonexistent. In addition, we have shown there is an optimum specimen-to-detector distance for annular configurations that maximizes their effective solid angle.

While the potential for these developments is exciting, there remains a challenge—namely to construct robust detectors that can operate under conditions that may also produce a large electron flux hitting the detector. These special geometries may require the return to the use of electron opaque windows like Be. The robustness of SDD systems against electron damage for ultrathin or windowless detectors has been reported, albeit sparingly (Barken et al., 2004), and further work in this area remains to be done.

Acknowledgments

This work was supported by the U.S. Department of Energy, Office of Science, at Argonne National Laboratory under contract DE-AC02-06CH11357

References

Barken, S., Saveliev, V.D., Iwanczyk, J.S., Feng, L., Tull, C.R., Patt, B.E., Newbury, D.E., Small, J.A. & Zaluzec, N.J. (2004). A new improved silicon multi-cathode detector (SMCD) for microanalysis and X-ray mapping applications, *Microsc Today* **12**, 36–38.

Bertuccio, G., Castoldi, A., Longoni, A., Sampietro, M. & Gauthier, C. (1992). New electrode geometry and potential distribution for soft-X-ray drift detectors. *Nucl Instrum Meth Phys Res A* **312**, 613–616.

Fitzgerald, R., Keil, K. & Heinrich, K.F.J. (1968). Solid-state energy-dispersion spectrometer for electron-microprobe X-ray analysis. *Science* **159**, 528.

Gatti, E. & Rehak, P. (1984). Semiconductor drift chamber—An application of a novel charge transport scheme. *Nucl Instrum Meth Phys Res* **225**, 608–614.

Goldstein, J.I., Newbury, D.E., Echilin, P., Joy, D.C., Romig, A.D., Lyman, C.E., Fiori, C. & Lifshin, E. (1992). *Scanning Electron Microscopy and X-ray Microanalysis*. New York: Plenum.

Iwanczyk, J.S.., Patt, B.E. & Segal, J. (1996). Simulation and modelling of a new silicon X-ray drift detector design for synchrotron radiation applications. *Nucl Instrum Meth Phys Res A* **380**, 288–294.

Kotula, P.G., Michael, J.R. & Rohde, M. (2008). Results from two four-channel Si-drift detectors on an SEM: Conventional and annular geometries. *Microsc Microanal* **14**(Suppl. 2), 116–117.

Zaluzec, N.J. (1979). Quantitative X-ray microanalysis. In *Introduction to Analytical Electron Microscopy*, Hren, J.J., Joy, D.C., & Goldstein, J.I. (Eds.), pp. 121–167. New York: Plenum Press.

Zaluzec, N.J. (2004). XEDS systems for the next generation analytical electron microscope. *Microsc Microanal* **10**(Suppl. 2), 122–123.